Correlations of crystal structure and solubility in organic salts: the case of the antiplasmodial drug piperaquine

Pietro Sacchi,[a] Laura Loconte,[b] Giovanni Macetti,[b] Silvia Rizzato[b,*] and Leonardo Lo Presti [b,c,d,*]

[a] School of Chemical Engineering and Analytical Science, University of Manchester, Manchester (UK)

[b] Department of Chemistry, Università degli Studi di Milano, Via Golgi 19, 20133 Milano (Italy)

[c] Centre for Materials Crystallography, Århus University, Langelandsgade 140, DK–8000 Århus (Denmark)

[d] Istituto di Scienze e Tecnologie Molecolari, Italian CNR, Via Golgi 19 I–20133 Milano (Italy)

* To whom correspondence should be addressed: leonardo.lopresti@unimi.it, silvia.rizzato@unimi.it

Abstract

Five organic salts of the antiplasmodial drug piperaquine (PQ, $C_{29}H_{32}Cl_2N_6$) were synthesized and characterized by X–ray diffraction methods. The corresponding solubilities in water and acetic acid solutions were evaluated in the 20 – 50 ºC (293 – 323 K) T range by UV–Vis spectroscopy, with the aim of elucidating how they depend on chemical, structural and thermodynamic factors. Experiments were complemented by DFT calculations, both *in vacuo* and in the solid state, to estimate changes in thermodynamic state functions related to the solvation process. It is demonstrated that solubility is mainly governed by electronic and chemical properties of the anion, while lattice energies and packing effects, including in–crystal conformational changes of the drug, play a less important role. PQ salts generally conform to the predictions of Hard and Soft Acid and Bases (HSAB) theory, as less soluble compounds bear ions of comparable hardness, and *vice–versa*. A remarkable exception, is the PQ hydrogen sulfate salt, whose poor solubility can be ascribed to an exceptionally stable crystal lattice. Other factors, such as entropic effects related to solid–state disorder, can influence the response of solubility to temperature.

1. Introduction

Piperaquine[1] (PQ, scheme 1) is a 4–aminoquinoline (4–AQ) antiplasmodial bearing two substituted 7–chloroquinoline moieties, connected by a double piperazinyl bridge.
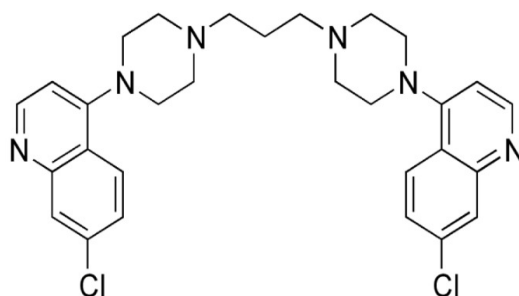
Scheme 1

To date, few investigations deal with the clinical pharmacokinetics of the sole PQ,[1–4] and no direct evidences even exist on its mechanism of action at the molecular level. The simpler and cheaper 4–AQ compound chloroquine[5,6] is often considered as a prototypical model for the action of drugs of this class. Thus, it is far more studied by both experimental[7–9] and computational[7,10,11] techniques, even though it is nowadays nearly ineffective due to specific resistance evolved by *Plasmodium falciparum*, the most aggressive and dangerous malaria parasite. On the contrary, in combination with artemisinin derivatives,[12] PQ is still employed worldwide in antimalarial multi–drug treatments.[1,13,14] Yet, parasites able to survive such therapies appeared in the last decade in Southeast Asia,[15,16] raising the urgent problem of continuously developing new strategies to win the race against the *Plasmodium* adaptability.

It is widely accepted that 4–AQ antimalarials interfere with the heme detoxification process in the acidic (pH $\cong$ 5) digestive vacuole (DV) of *Plasmodium* protozoa.[17] It is believed that their target is the heme molecule, either in the form of Fe(III)protoporphyrin in solution,[5–7] or at the surface of growing hemozoin crystals.[18] The structure of the heme–drug adduct, however, is still debated. Relevant actors in the recognition process should be (i) $\pi \cdots \pi$ stacking interactions between the quinoline core of the drug and the heme pyrrolic subunits,[8,9] perhaps associated to (ii) a direct coordinative Fe–N bond involving quinoline nitrogen atoms.[6,19] Also (iii) charge–assisted hydrogen bonds (CAHBs) involving the aliphatic amines of the 4–AQ system as donors might play a role.[5]

When PQ comes into play, the problem is complicated by the large conformational freedom of the hydrocarbon bridge connecting the two aminoquinoline moieties (Scheme 1), which in principle could allow different interaction modes with respect to less flexible drugs of the same class. Moreover, the title compound bears four basic amine functions, with pKa = 6.88, 6.24 (tertiary N)

and 5.72, 5.39 (quinoline N).[20] Thus, in the acidic DV, the main forms in equilibrium are H_3PQ^{3+} and H_4PQ^{4+}, with a slight preference for the fully protonated one (Figure S1 SI).

Beyond the mechanism of action of a medical drug, it is well known how its solubility and dissolution rate as well as other physical (appearance, density and hygroscopicity, thermodynamic stability) and chemical (integrity and labelled potency) properties can change dramatically with the solid form (salts, polymorphs, solvates, co-crystals, amorphous forms). It follows that, the chemical form and the solid phase of a pharmaceutical ingredient can have a great impact on the bioavailability and the overall stability of the drug but also on the convenience in production and storage of the final product. Since most of the drug molecules, like PQ, are either weak acids or bases, that is, possess ionic sites in their molecule, salt formation represents a useful and simple chemical way to modify the properties of the drug substances.[21] However, in a salt screening study the choice of a salt, and the salt formation feasibility, is largely ruled by acid-base chemical aspects, toxicological implications, dosage form considerations, pharmacological indications and marketing preferences.[22,23] Many organic counterions and some of the common inorganic ions (i.e. calcium, phosphate, chloride) show a very good tolerability and a low toxicity because are components of food, natural constituents of the body or involved in the metabolic cycles. For many other anion species, specific remarks must be addressed.

It must be made clear that, according to medicinal evaluation authorities, different salt forms are not bioequivalent or exchangeable. In fact, albeit rare, counterions can lend an additional therapeutic action to the active ingredient or modify the toxicity of the parent compound, influence the formulation characteristics, change the release properties and the delivery mechanism.

At present, the number of acceptable salt formers, deemed as harmless components, is quite reduced and the choice is essentially limited to a list of counteranions categorized in three classes based on a toxicity criteria[23,24] (Class 1: no restrictions to use, physiological and metabolic ubiquitous ions; Class 2: limited use, not natural ions, low toxicity; Class 3: occasionally use, not natural ions, secondary effects). A regulatory guidance for the acceptance of new salt forms of already approved active ingredients is still yet available.

The neutral form of lipophilic PQ,[3] (Section S2.1 SI) is not soluble in water as well as the salt from (hydrogen phosphate tetrahydrate) mainly used in the commercial formulations[25] that results in a reduced oral bioavailability of the drug.[2] Investigating which factors govern the solubility of PQ is therefore interesting in the context of developing new and more advantageous formulations. To date,

however, systematic studies on the possibility of enhancing the solubility of piperaquine salts are lacking.

In the present work, our goal is to understand how chemical and crystallographic factors are intertwined in determining the solubility of PQ salts. At the same time, we investigate how different non–covalent interaction (NCI) networks govern molecular conformation and packing in the solid state. To synthesize new PQ–based compounds, to be compared with the phosphate tetrahydrate one, four acid system are considered as salt-former, that is, sulfate (ordinary, class 1), bromide and nitrate (less common, class 2) and triflate (uncommon). Though the therapeutic use of their salts cannot be excluded a priori, nitrate and triflate have been chosen only on a chemical basis to span as widely as possible the landscape of structure–properties relationships. This is because nitrate anion has always been considered as both a toxic constituent of the diet, strictly regulated in water and food, and an inert specie endogenously generated from nitrogen monoxide (NO).[26] However, due to its recognised adverse physiological effects, nitrate ion is generally not recommendable, although not prohibited, for salt conversion of drugs.[27] For the triflate base, no biological or physiological data are available. An in-silico approach to define potential toxicity problems and assess the safety of triflate and other potential inorganic and organic ionic components in pharmaceutical medicaments could be performed, even though a clear general predictive model in computational toxicology is not yet available.[28,29]

2. Methods

2.1 Synthesis. Reagent–grade chemicals ($\geq$ 98% purity) were purchased from Sigma Aldrich and used without further purification. 1,3–bis[4–(7–chloroquinolin–4–yl)piperazin–1–yl]propane (piperaquine) tetraphosphate tetrahydrate (PPT) salt was directly employed for UV–vis measurements (see below). All the other compounds were obtained according to the following procedures.

2.1.1 Neutral PQ. ~ 1 g of commercial PPT was dissolved in 40 mL of aqueous acetic acid 10 M. Concentrated aqueous NH_3 was added dropwise under continuous stirring up to pH = 8. The precipitation of neutral PQ started at pH = 6. The powder was filtered, washed with deionized water and dried in oven at 40°C. The structure was confirmed by powder X-ray diffraction (XRPD) and was identical to that recently reported by Wang *et al.*.[30] X–ray quality single crystals were grown from $CHCl_3$ by slow evaporation at room temperature.

2.1.2 PQ tetraphosphate tetrahydrate $((H_4PQ^{4+})(H_2PO_4^-)_4 \cdot 4H_2O$, PPT$)$. X–ray quality single crystals were obtained upon recrystallization of commercial PPT (0.2778 g) from 1 M aqueous acetic acid (20 mL). The solution was placed in a Petri dish ($\varnothing$ 50 mm) and left free to evaporate overnight at room temperature (RT).

2.1.3 PQ hydrogen sulfate hydrate $((H_4PQ^{4+})(HSO_4^-)_5 \cdot nH_2O \cdot H_3O^+$, PHS$)$. 0.3075 g of commercial PPT were put into 70 mL of aqueous 1 M H_2SO_4 in a glass flask. 5 mL of concentrated H_2SO_4 were added and the suspension heated under continuous stirring at 55°C (328 K) until complete dissolution. After cooling down to room temperature, the solution was poured in a Petri dish ($\varnothing$ 100 mm) and left free to evaporate overnight. Eventually, plate–like red PHS crystals suitable for the single crystal X–ray analysis were obtained. An equivalent synthetic route consists in dissolving 0.4306 g of neutral piperaquine (§ 2.1.1) into 105 mL of aqueous H_2SO_4 10 M and leaving the solution free to evaporate in a Petri dish ($\varnothing$ 60 mm) at room temperature. After ~ 2 months, plate–like crystals of PHS were filtered, dried and ground in a mortar. The identity of the material was confirmed by XRPD ; UV–vis measurements were performed on the ground powder (see below).

2.1.4. PQ triflate trihydrate $((H_4PQ^{4+})(CF_3SO_3^-)_4 \cdot 3(H_2O)$, PTT$)$. 0.4312 g of neutral PQ (§ 2.1.1) were put into 16 mL of aqueous trifluoromethanesulfonic acid (CF_3SO_3H) 4.2 M. Complete dissolution was obtained only by adding 34 mL of supplementary acetic acid 10 M. Then, the solution was poured in a Petri dish ($\varnothing$ 60 mm) and left free to evaporate in air at room temperature. After ~ 1 week, several small crystals appeared; in ~ 2 weeks, well–formed, transparent and colorless prisms were present. Some specimens were selected for single–crystal X–ray diffraction, and the remaining material ground in a mortar to perform solubility measurements (see below).

2.1.5. PQ bromide trihydrate $((H_4PQ^{4+})(Br^-)_5 \cdot 3H_2O \cdot H_3O^+$, PBT$)$. 0.0508 g of neutral PQ (§ 2.1.1) were added to 8 mL of HBr in acetic acid (32%) and 3 mL of distilled water. The suspension was stirred until complete dissolution, poured into a 25 mL glass flask and left free to evaporate in air at room temperature. Upon resting, the solution became immediately cloudy; very small crystals quickly formed on the internal glass surfaces of the flask. The precipitate was filtered, added to 5 mL of CH_3COOH 10 M and stirred until complete re–dissolution. After ~ 1 month, prismatic crystals formed by slow evaporation at room temperature. One of them was selected for the X–ray analysis, and the remaining material ground into a powder for the UV–vis measurements.

2.1.6. PQ nitrate $((H_4PQ^{4+})(NO_3^-)_4 \cdot (HNO_3)_3$, PN$)$. 0.4707 g of neutral PQ (§ 2.1.1) were added to 30 mL of aqueous HNO_3 9.5 M. Complete dissolution was achieved only after the addition of 65% nitric acid up to a final volume of 65 mL. The solution was left free to evaporate at room

temperature in a Petri dish (∅ 80 mm). After 6 days, only one large crystal of PN had appeared. Smaller crystals formed in subsequent days, but tended to dissolve spontaneously. When the first specimen was almost 1 cm long, a couple of smaller crystals began to steadily grow. One of the latter was selected to undergo X–ray diffraction. The rest of the material was ground in a mortar to be investigated by means of XPRD and UV–vis techniques (see below).

Table 1. Crystallographic and refinement details of hydrogen phosphate (PPT), hydrogen sulfate (PHS), triflate (PTT), bromide (PBT) and nitrate (PN) salts of fully protonated piperaquine (H_4PQ^{4+}).

Substance	PPT	PHS	PTT	PBT	PN
Temperature / K	150(2)	120(2)	298(2)	120(2)	296(2)
Crystal data					
Formula	(H_4PQ^{4+}) $(H_2PO_4^-)_4 \cdot 4 \cdot H_2O$	$(H_4PQ^{4+})(HSO_4^-)_5$ $6.6 \cdot H_2O\ H_3O^+$	(H_4PQ^{4+}) $(CF_3SO_3^-)_4 \cdot 3 \cdot H_2O$	$(H_4PQ^{4+})(Br^-)_5$ $3 \cdot H_2O\ H_3O^+,$	(H_4PQ^{4+}) $(NO_3^-)_4\,(HNO_3)_3$
Z, Z' [a]	4, 1	4, 1	8, 1	1, 0.5	2, 1
Space group	$P2_1/n$	Cc	$C2/c$	$P{-}1$	$P{-}1$
a / Å	22.276(1)	21.4922(7)	19.031(4)	7.4928(2)	11.250(6)
b / Å	7.4516(4)	7.3576(2)	18.208(4)	14.3820(4)	13.6923(8)
c / Å	27.897(1)	29.6485(10)	16.149(3)	17.6634(4)	14.6995(9)
α / deg	90.	90.	90.	88.936(1)	68.320(1)
β / deg	107.385(1)	101.563(2)	118.92(3)	80.414(1)	84.958(1)
γ / deg	90.	90.	90.	84.701(1)	83.067(1)
V /Å^3	4419.2(4)	4591.7(2)	4898(2)	1853.11(8)	2081.8(2)
Density / g·cm^{-3}	1.490	1.662	1.604	1.814	1.558
μ / mm^{-1}	0.373	0.469	0.417	5.608	0.255
Data collection					
Measured reflns	55499	31452	42406	27494	31574
Unique reflns.	10187	10564	5631	8522	11874
Obs. ($I{>}2\sigma(I)$) unique reflns	7792	10194	4580	7721	9244
Completeness / %	100.0	100.0	100.0	99.9	99.3
R_{int}	0.033	0.015	0.024	0.019	0.019
Refinement					
Max resolution / Å	0.769	0.769	0.769	0.769	0.714
$R(F)$, $I > 2\,\sigma(I)$	0.058	0.042	0.059	0.020	0.046
$wR(F^2)$, all	0.178	0.122	0.187	0.048	0.136
Goodness–of–fit	1.044	1.044	1.047	1.007	1.037
$\Delta\rho_{MAX}, \Delta\rho_{MIN}$ / e·Å^{-3}	1.220, –0.654[b]	0.608, –1.000 [b]	0.557, –0.611	0.573, –0.684	0.394, –0.477

[a] Z: Number of chemical formulae of piperaquine in the unit cell; Z': $Z/mult$, where *mult* is the crystallographic multiplicity of the general position.
[b] Large Fourier residuals in the PPT and PHS structures are due to highly disordered chemical species. See Sections S2.3 and S2.4 in the Supplementary Information for a full discussion of disorder.

2.2 Single–crystal X–ray diffraction (SCXD). SCXD experiments were carried out on a Bruker Smart three–circle diffractometer equipped with an Apex II CCD detector and an Oxford Cryosystem 600 nitrogen blower. Graphite–monochromated Mo Kα radiation ($\lambda = 0.71073$ Å) at a nominal power of 50 kV x 30 mA was used in conjunction with a ω–scan collection strategy at

variable time intervals (20–40 s/frame) and steps of 0.5 deg. All the experiments were performed in controlled temperature conditions between 100(2) K and 296(2) K, with maximum resolution in the 0.71–0.77 Å^{-1} interval of sinθ/λ and completeness ranging from 99.3 % to 100.0 % (Table 1). SAINT+[31] and SADABS[32] programs were employed, respectively, for data reductions and either empirical (PQ, PPT, PHS, and PN) or analytical (PTT and PB) absorption corrections. The structures were solved by direct methods and refined within the spherical atom approximation with the least–square procedure implemented in the Shelx suite of codes.[33] Geometries of hydrogen atoms were idealized, and riding–motion restraints (HFIX n3) applied throughout. All the X–H bond distances (X = C, N, O) were renormalized *a posteriori* to neutron–derived estimates[34] by Mercury v3.9.[35] Table 1 below summarizes relevant crystallographic details, while Section S2 SI provide full information on the main features of the crystal packing of the various structures.

2.3 Solubility measurements. The solubility of the PQ salts was measured at intervals of 5°C in the 20°C – 50°C range of *T* by means of UV-vis spectroscopy. A procedure similar to that detailed by Daneshfar *et al.*[36] was adopted throughout. Each powdered compound was put in a small glass flask with a minimum amount of reagent–grade water and kept at the desired temperature for 2 hours under continuous stirring. A Huber circulation thermostat CC-205B was employed, exploiting a precision of ± 0.1 K. Then, stirring was stopped and the suspension left free to rest at constant temperature for 30 minutes. Samples of 20 μL (10 μL for PN) were harvested from the liquid near the surface and diluted in 10 mL of either reagent–grade water or acetic acid 1 M within a volumetric flask. The acetic acid guarantees the quantitative solubilization of the drug and thus tests in acidic solutions are useful benchmark against the actual solubility in water. The UV–vis absorbance of these solutions was measured immediately at 349 nm in H_2O and at 344 nm in acetic acid.

Absorbance measurements were performed in the 200–800 nm range at a scan rate of 1 nm/s with a Beckman Coulter DU–800 spectrophotometer equipped with D_2 and tungsten sources. The maximum error on the measured absorbance should be lower than 0.005. Quartz cuvettes with optical length of 1 cm were used throughout.

2.4 Quantum simulations. Single–point periodic DFT calculations were carried out starting from the experimental structures of the synthesized compounds (Section 2.2) with the CRYSTAL14 program[37] to retrieve information on the lattice energies. The Minnesota–class meta–GGA M06 functional[38] was used in conjunction with basis sets taken from the CRYSTAL library[39–44] and optimized for solid–state calculations. Truncation criteria of the Coulomb and exchange series were set either to 10^{-8} or 10^{-16} (TOLINTEG 8 8 8 8 16). A level shifter of 0.3 h and a 80 % mixing of the

Kohn–Sham matrix coefficients were applied to subsequent SCF cycles to accelerate convergence.[37] A 4 x 4 x 4 sampling of the independent part of the first Brillouin zone defined the k–space grid where the SCF problem is iteratively solved. In disordered structures (Section S2 SI), preliminary partial geometry optimizations were carried out to determine the uncertain positions of hydrogen atoms, typically belonging to co–crystallized solvent. Only disordered sites with the highest occupation factors were modelled. More details are given in Section S3 SI.

Crystal cohesive energies, E_{coh}, are defined as:[45–49]

$$E_{coh} = E_{bulk} - \sum_{i=1}^{n} \left(E_{iso,i} + \Delta E_{rel,i} - \Delta E_{BSSE,i} \right) \tag{1}$$

The summation runs over the n molecules in the unit cell, whose total electronic energy is E_{bulk}; $E_{iso,i}$ is the energy of the i–th molecule extracted from the crystal (keyword[37] MOLECULE), frozen at its solid–state conformation. The negative $\Delta E_{rel,i}$ term accounts for the relaxation energy, *i.e.* for the energy difference between a molecule fully relaxed *in vacuo* and the same molecule at its solid–state geometry. Eventually, $\Delta E_{BSSE,i}$ is the positive correction for basis set superposition error of the i–th molecule according to the counterpoise method by Boys & Bernardi,[50] here applied within a maximum cutoff distance of 6.5 Å.

Isolated molecules were also simulated with the Gaussian09 program.[51] The same basis set used in solid–state calculations was exploited in conjunction with a DFT B3LYP hamiltonian, exploiting experimental solid–state geometries as references. *In vacuo* calculations provide (i) relaxation terms, ΔE_{rel}, to crystal cohesive energies; (ii) reasonable estimates of chemical hardness of the anions, η, which can be computed as η = ½ ($\varepsilon_{HOMO} - \varepsilon_{LUMO}$) once the energies of the frontier orbitals, ε_{HOMO} and ε_{LUMO}, are known, under the assumption that the Koopmans' theorem holds true; (iii) hydration energies of individual molecular ions (see Section 4). To this end, the solvent was implicitly simulated within the Polarizable Continuum Model (PCM) formalism, exploiting the Solvation Model based on Density (SMD) variation of Truhlar,[52] which is recommended when dealing with solvation thermodynamics.[51] Finally, simulations on isolated H_4PQ^{4+} molecular pairs frozen at their experimentally–derived geometries were carried out to estimate the stabilizing contributions due to π···π stacking interactions, according to the procedure detailed in Section S4 SI.

2.5 Quality assessment and reproducibility. Processing of diffraction data and quantum simulations were performed using commercial programs. Full details on the refinement procedure are deposited in the Supporting Information (Section S2 SI). CCDC 1882786-1882791 contain the

supplementary crystallographic data for this paper. These data can be obtained free of charge from The Cambridge Crystallographic Data Centre via www.ccdc.cam.ac.uk/structures.

3. Results

3.1 Comparison of the H₄PQ⁴⁺ salt structures. Detailed descriptions of the packing modes of the synthesized salts (PPT, PHS, PTT, PBT and PN) are deposited in the SI (Section S2). Figure 1 shows the Hirshfeld surface fingerprint plots[53] of the various H_4PQ^{4+} ions in different crystalline environments, as computed by the CrystalExplorer[54] suite of programs. They share a general similarity in the overall shape, indicating that most key crystal packing features are recurrent, but differ in finer details, reflecting specific peculiarities of the different NCI networks. The similarities among different PQ salts are particularly relevant in this context: we expect that conserved NCI are most likely due to true structure–determining factors.
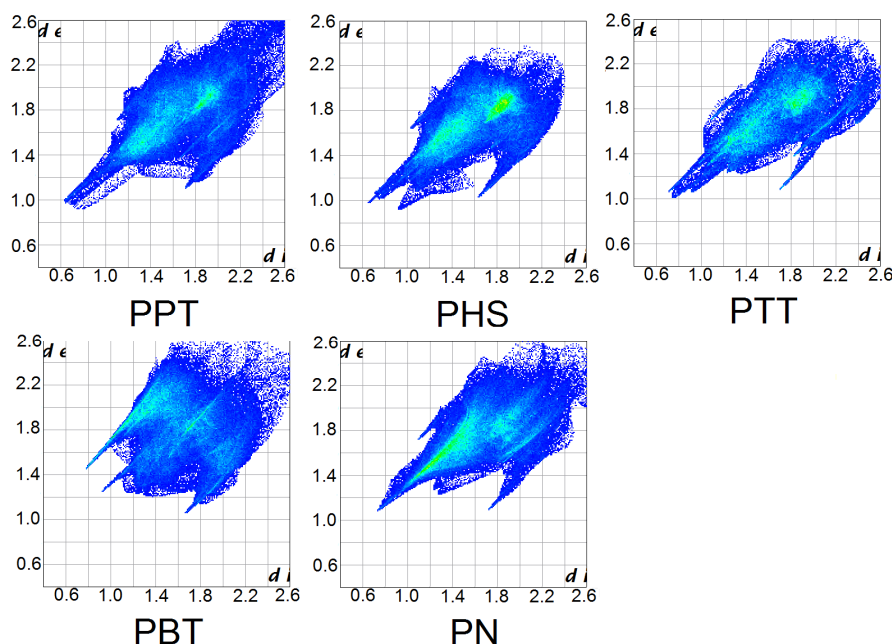
Figure 1. Hirshfeld surface fingerprint plots of PPT (hydrogen phosphate), PHS (hydrogen sulfate), PTT (triflate), PBT (bromide) and PN (nitrate) salts of piperaquine.

First, all the fingerprint plots are markedly asymmetric, indicating that H_4PQ^{4+} does not preferentially set up close contacts with symmetry images of itself. Rather, PQ cations tend to be surrounded by anions, as expected in organic salts. With the only exception of the bromide compound (PBT), a very long and broad spike is always apparent in the lower left part of the diagram, representative of strong $NH^+ \cdots O^-$ CAHBs at very short ($d_i + d_e \approx 1.6–1.8$ Å) $H \cdots O$ contact distances.

In general, all the 4 N–H functions in protonated piperaquine are generally involved in close contacts with anions; only in the PTT salt, the aliphatic NH^+ groups are connected with two neutral water molecules, while triflate anions prefer to approach quinoline NH^+ donors. This is likely due to the higher dimensions of $CF_3SO_3^-$ ions, which result in a reduced accessibility of the cation in the more sterically crowded regions of the aliphatic nitrogen atoms, while the piperaquine molecule exploits here a less extended conformation (see Section 3.2 below). Accordingly, H_4PQ^{4+} in PTT sets up only two CAHB interactions per molecule, to be compared with the four CAHBs formed in the other salts here considered.

Second, a pronounced spike is also evident in PHS at short $d_i \approx d_e \approx 0.8–0.9$ Å along the main diagonal. A similar feature, though less marked and shifted at longer $d_i + d_e$, is also present in the nitrate PN salt. They are both the signature of ubiquitous close H···H contacts, which in PHS include very short ones (< 2 Å) that arise due to the closeness of co–crystallized water molecules.

Third, all the fingerprint plots also share a similar spike at $d_i + d_e \approx 2.7$ Å, in the lower right part of the plane. This originates from CH(piperazine ring)···Cl contacts in which PQ plays the role of the acceptor. In fact, it is mirrored by an analogue feature in the upper left part of the diagram, in most cases partly covered by the CAHBs signature, which accounts for the same interaction from the donor's viewpoint. Another interesting region is the one located at $d_i \approx d_e \approx 1.8$ Å along the main diagonal, which it always bear a significant contact frequency and signals the occurring $\pi \cdots \pi$ contacts among flat rings. Some differences emerge as well, though. Such interactions are more frequent in the sulfate salt (PHS), where "sandwich–like" arrangements among neighboring quinoline rings are the preferred stacking mode (Section S2.4 SI). This is in agreement with geometrical and energetic parameters computed for these stacking interactions (Table S7 SI).

In the bromide structure (PBT), the signature of stacking interactions is barely apparent in the fingerprint plot (Figure 1) and, accordingly, it does not provide significant contributions to the lattice stabilization (Tables S7 and S8 SI). On the contrary, a bright veining runs along the main diagonal of the diagram, marking Cl···Br contacts with bromide ions. Other differences concern the hydrogen bond pattern. According to Shannon,[55] the effective ionic radius of Br^- is 1.96 Å, *i.e.* it has larger dimensions than an oxygen acceptor, but at the same time it is significantly smaller than any other molecular anion considered in this work. Thus, $H^+ \cdots Br^-$ contacts are longer than the $H^+ \cdots O^-$ ones, and appear in the fingerprint plot as a sharp and brilliant spike at minimum $d_i + d_e \approx 2.2$ Å in the upper left region of the diagram. A secondary, parallel spike also appears at a similar $d_i + d_e$, but shorter than

the first one and translated toward greater d_i's, which is due to weaker CH···O contacts involving water oxygen atoms.

3.2 In–crystal conformation of PQ. The packing differences described in Section 3.1 are intertwined with the conformational freedom of the PQ molecule. Indeed, the title compound can easily undergo conformational changes to fit specific packing requirements, according to the chemical nature and arrangement of anions and water in the lattice. Figure 2 sketches the main rotatable bonds and groups in PQ. The puckering state of the piperazinyl substituents has no effect, as the only detected conformer is the chair–like one (see Section S5 SI).
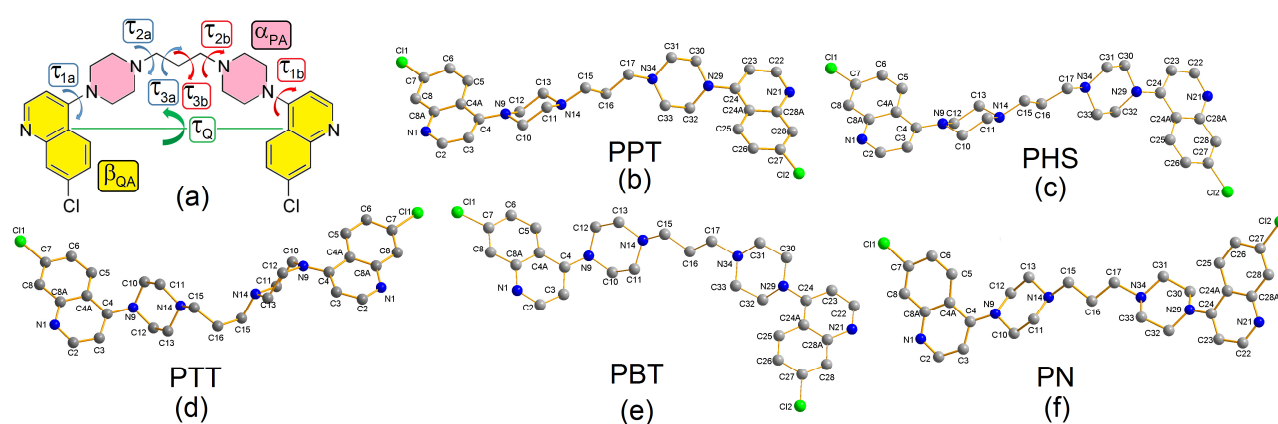
Figure 2. (a) Main torsional conformational descriptors of PQ. α_{PA} and β_{QA} are the angles between the piperazine (pink) and the quinoline (yellow) mean planes. (b–f) Structures of PQ molecular ions as found by X–ray crystallography in the phosphate (b), hydrogen sulfate(c), triflate (d), bromide (e) and nitrate (f) salts. Hydrogen atoms are omitted for clarity. Atom labels are indicated.

The τ_1, τ_2 and τ_3 torsion angles (Figure 2, Table 2) determine the general conformation of the H_4PQ^{4+} ions and, in particular, the overall molecular symmetry. In PTT, half of a PQ molecule is symmetry–dependent on the other half through a C_2 axis passing through the C16 methylene group in the mid of the hydrocarbon $-(CH_2)_3-$ linker (Section S2.5 SI). Thus, τ_{1a}, τ_{2a} and τ_{3a} are identical to the corresponding descriptors, τ_{1b}, τ_{2b} and τ_{3b}, of the symmetry–related fragment. Increasingly larger differences between these two sets of torsions imply significant asymmetries. Interestingly, three out of five crystal structures bear H_4PQ^{4+} moieties in fully symmetric (PTT) or almost symmetric (PPT and PHS) arrangements (Table 2). In PHS, despite the absence of any symmetry element within the molecule, the two sets of torsions remain identical; in PPT, the only significant difference concerns a $\approx +15°$ opening of τ_{2b} with respect to τ_{2a}. In the PBT and PN structures, on the contrary, the two

sets of dihedrals are no longer similar, with τ_{2b} wider than τ_{2a} by more than 100°, and $\tau_{3b} \approx -\tau_{3a}$. Different settings of the τ angles often imply a change in the mutual orientation of the quinoline rings, as it can be appreciated by looking at the terminal C–Cl bonds in Figure 2. Being τ_Q the angle between the quinoline moieties, defined through the atom sequence C4A–C4–C24–C24A (Figure 2), $\tau_Q > 90°$ or $\tau_Q < -90°$ indicate an "anti" conformer (PPT, PHS and PBT), whereas $-90° < \tau_Q < +90°$ implies a "syn" one (PTT and PN). The dihedral angle β_{QA} between the mean least–squares planes of the quinoline C–N backbones provides further insights. Values of β_{QA} close to zero imply that the two quinoline rings are almost parallel to each other; if also the absolute $|\tau_Q|$ dihedral is small, they lie almost exactly on the same plane. This is the case of the nitrate structure, PN, where the PQ ions are essentially "flat" due to symmetry constraints. On the contrary, in PBT and PTT, large $|\tau_Q|$ and small β_{QA} imply that the two aromatic systems are parallel, but do not lie on the same plane, setting up a sort of "ladder" conformation. In PHS and PPT, eventually, quinoline groups are tilted ($\beta_{QA} > 20°$), determining the preference for a "vane mill" conformation. Interestingly, the latter conformer is invariably associated to the energetically most favorable stacking arrangements in PPT and PHS (Section S4 SI).

Table 2. Conformational descriptors of piperaquine cations in hydrogen phosphate (PPT), hydrogen sulfate (PHS), triflate (PTT), bromide (PBT) and nitrate (PN) salts. Estimated standard deviations are given in parentheses.

Structure	τ_{1a}/τ_{1b} [a]	τ_{2a}/τ_{2b} [a]	τ_{3a}/τ_{3b} [a]	τ_Q [b]	β_{QA} [c]	d_{NN} [d]	α_{PA} [e]
PPT	−10.9(4)/−12.7(4)	156.8(2) /172.2(2)	176.9(2) /172.7(2)	−163.3(2)	20.9	5.036(3)	79.7
PHS	−13.3(5)/−13.6(5)	167.1(3) /167.0(3)	−174.2(3) /−174.8(3)	−143.7(2)	40.5	5.019(4)	78.9
PTT	−135.5(4) /−135.5(4)	−173.4(2) /−173.4(2)	66.6(3) /66.6(3)	−52.8(3)	7.2	3.977(3)	74.0
PBT	20.7(2) / −13.8(2)	55.4(2) / 170.8(1)	172.8(1) /−176.7(1)	126.2(3)	6.6	5.017(2)	14.4
PN	−10.1(2) / −137.0(2)	65.8(2) / 166.0(1)	163.8(1) /−165.3(1)	−2.3	6.8	4.961(2)	22.9

[a] Dihedral angles (deg) describing the mutual orientations of rotatable bonds (see Figure 2). τ_{1a}/τ_{1b} correspond to the atom sequence C3–C4–N9–C10 / C23–C24–N29–C30, τ_{2a}/τ_{2b} to C11–N14–C15–C16/C33–N34–C17–C16 and τ_{3a}/τ_{3b} to N14–C15–C16–C17 / N34–C17–C16–C15.
[b] Dihedral angle (deg) expressing the mutual tilting of the quinoline moieties through the C4A–C4–C24–C24A atom sequence.
[c] Angle (deg) between the least square planes of the quinoline backbones. It describes whether they are planar or not.
[d] Distance (Å) between the protonated piperazine N atoms. It describes how much the structure is compact or stretched.
[e] Angle (deg) between the piperazine backbone least squares planes.

Another useful descriptor of the overall folding is the distance between the piperazine N atoms, d_{NN}, across the central hydrocarbon $-(CH_2)_3-$ linker. To the sake of comparison, in crystalline pentane (CSD refcode: PENTAN01), where neighboring methylene groups are almost perfectly antiperiplanar, the two terminal $-CH_3$ groups lie 5.072 Å apart. While in PPT, PHS, and PBT the

hydrocarbon linker is fully extended, H_4PQ^{4+} ions assume a sort of bent conformation at least in PTT, where $d_{NN} \approx 3.9$ Å, and possibly in PN, with $d_{NN} \approx 4.9$ Å (Table 2). The angle between the piperazine ring mean planes (α_{PA}), finally, can give an indication of the mutual orientation of the aliphatic N–H groups involved in hydrogen bonding (see Section S2 SI). When this descriptor is relatively small (<60°), N–H bonds are oriented in the same direction, with the dihedral angle defined by the atom sequence H14–N14···N34–H34 as low as –9(2)° (PBT) or –6(2)° (PN). On the contrary, α_{PA} >60° implies that aliphatic N–H groups are mutually orthogonal to each other, the same dihedral being as large as 90(3)° (PPT), 96(2)° (PHS) and 92(4)° (PTT). It is easy to see that α_{PA} correlates with τ_Q, *i.e.* molecules with an anti– (syn–) conformation also bear collinear (orthogonal) N–H groups. However, the main features of the hydrogen bond patterns, such as the ability of setting up strong CAHBs (Section 3.1), are qualitatively conserved independent on the piperaquine conformation.

3.3 Solubility of PQ salts. Figure 3 shows the estimates for the solubilities (S) of the PQ salts as a function of T, referred to wavelengths of 349 nm in H_2O and of 344 nm in acetic acid (Section 2.3). These were selected according to the maxima found during the calibration procedure; the interested reader can find full details in Sections S6 and S7 SI. All the compounds show an exponential dependence on T. Solubilities in an acidic environment are slightly larger than in water, likely due to the different ionic strength of the resulting solution (Figure 3b and Tables S11–S12 SI). However, the difference is barely appreciable and in the subsequent thermodynamic analysis, the average S estimates were employed. Upon linearization (Figure S9 SI), the least–squares fittings based on the functional form $\log_{10}S=m \cdot T–q$, S being the solubility and T the temperature, give identical m and q parameters in both solvents within the statistical tolerance of 1–3 estimated standard deviations (Table S13). The highest solubility is invariably associated to the bromide salt (PBT). At 20 °C, the latter is ten times more soluble than PHS and almost two times more soluble than PPT. Moreover, S(PBT) increases faster than all the other compounds, and escalates by roughly 740 % on going from 20 °C to 50 °C (293 – 323 K). At $T = 20$ °C, the solubilities of the other salts follow the sequence S(PHS) << S(PPT) < S(PTT), and this order is strictly conserved up to 50 °C. The nitrate PN, on the contrary, behaves quite differently, as the corresponding curve has a slope comparable with that of PBT. As a consequence, PN bears at $T = 20$ °C a solubility comparable with that of least soluble hydrogen sulfate, PHS; then, S(PN) quickly increases, until it crosses the curves of PPT ($T >$ 35 °C, 308 K) and even PTT ($T > 40$ °C, 313 K). Clearly, this process is slightly faster in AcOH 1 M. No other curve shows a similar behavior, which may be related to the fact that PN, at variance with

most of the other crystal structures here examined, does not bear disordered co–formers its lattice (see Section S2.7 SI and Section 4 below).
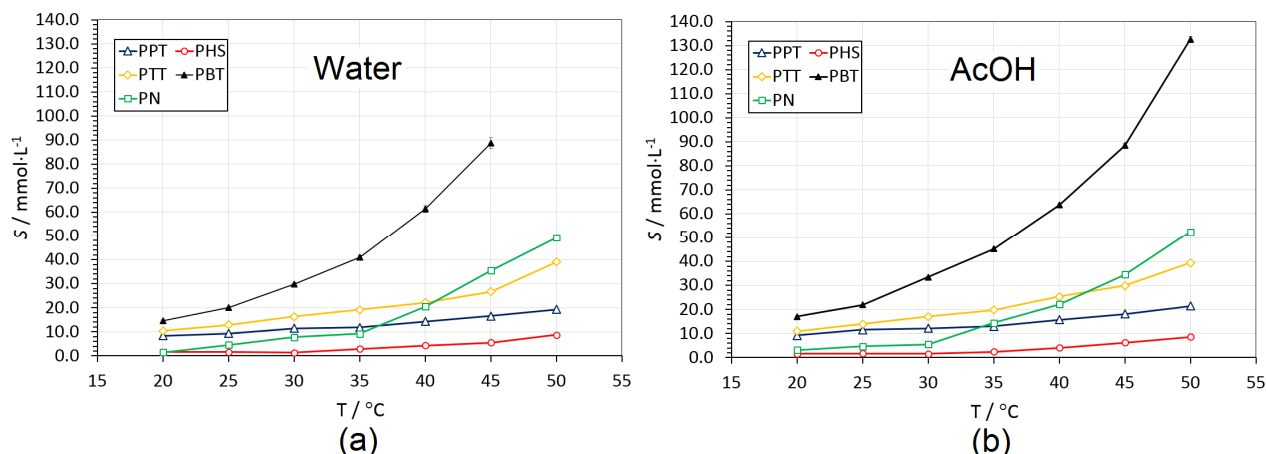
Figure 3. Solubility curves of PQ salts (PPT: hydrogen phosphate, open triangles; PHS: hydrogen sulfate, circles; PTT: triflate, diamonds; PBT: bromide, full triangles; PN: nitrate, squares) as a function of *T*. Vertical bars correspond to 1 estimated standard deviations (e.s.d.'s); in most cases, they are smaller than the dimension of the corresponding experimental point. Full broken lines serve just as a guide for the eye. (a) Measurements in water. (b) Measurements in AcOH 1 M.

3.4. Hydration. Solubility is usually related to the lattice energy, and thus to relevant non–covalent interactions among the molecules in the crystalline state.[56] Accordingly, it can be correlated, though not exclusively, to the melting point.[57] However, solute–solvent interactions and entropic effects in solution[58] are important as well, implying that no obvious rules exist that allow predicting the solubility of a given compound just from the sole knowledge of its crystal structure. The problem is further complicated in co–crystals and molecular salts, which contain more than one chemical specie.[59] Even though it has been claimed that in multicomponent systems the lattice energy is determinant to rationalize the solubility,[56] this is not the case for PQ salts. In agreement with previous studies,[59] crystal cohesive energies, E_{coh} (Table S14 SI), of the title compounds do not correlate with the measured solubilities (Figure S11 SI). To take into account explicitly solvent effects, Gibbs free hydration energies, ΔG^{*}_{hyd}, were estimated by quantum simulations in a polarizable continuum environment (Section 2.4). Thermodynamic state functions are derived from the corresponding electronic energies through the knowledge of the corresponding partition functions,[60,61] assuming that each chemical specie behaves as a perfect gas. The superscript (*) here follows the Ben–Naim & Marcus[62] terminology and implies the transfer of molecules between two phases at a fixed centres of mass in each phase. We assessed the accuracy of the method on the same test cases suggested by Misin *et al.*[63] (Table S15 SI), finding that it was fully comparable to that achieved by other recipes,

even though our predictions for the hydration energies of the anions are underestimated to a certain extent (Table 3).

Table 3. Hydration free energies (kJ·mol^{-1}) of ions contained in PPT, PHS, PTT, PBT and PN piperaquine salts.

Salt	Ion	N_A/N_{PQ}[a]	ΔG^*_{hyd}, expt.[b]	ΔG^*_{hyd}, calc.	$\Delta G_{hyd,tot}$ calc.[c]
PPT	H_4PQ^{4+}	1	–	–2110.3	–2110.3
	$H_2PO_4^-$	4	–465	–314	–1256
PHS	H_4PQ^{4+}	1	–	–2110.3	–2110.3
	HSO_4^-	4	–	–291 ⎫	–2199
	SO_4^{2-}	1[d]	–1080	–1035 ⎭	
PTT	H_4PQ^{4+}	1	–	–2125.0	–2125.0
	$CF_3SO_3^-$	4	–	–232	–928
PBT	H_4PQ^{4+}	1	–	–2117.8	–2117.8
	Br^-	5	–315	–226	–1130
PN	H_4PQ^{4+}	1	–	–2107.6	–2107.6
	NO_3^-	4	–300	–276	–1104

[a] Ratio between the number of ions and the number of piperaquine molecules in the asymmetric unit

[b] Experimental data, when available, where taken from ref. [64].

[c] Total ΔG^*_{hyd} estimates, from the sum of all the contributions of ions with the same charge in the asymmetric unit.

[d] The contribution of a single sulfate ion must be taken into account here, as the optimization of disordered hydrogen atoms predict a proton transfer between a HSO_4^- ion to a neutral water molecule (Section S3 SI).

Table 3 reports the results for H_4PQ^{4+} species and their anions in the various salts. As expected, the hydration free energies of the cations are very similar to each other. Differences not exceeding 18 kJ·mol^{-1} reflect the conformational differences of the molecular ions in the various crystal structures (Section 3.2), with a standard deviation of ≈ 0.3 % with respect to the mean ΔG^*_{hyd} estimate. In any case, these differences are likely too small to account for the significant changes in solubility across the series of salts here examined (Section 3.3), which should be thus ascribed to the respective counterions. We note that, interestingly, the sulfate salt, whose anion sets up the most favourable interaction with water, is also the one with the lowest solubility.

3.5. Thermodynamic cycle of solvation. From a thermodynamic viewpoint, the solvation reaction can be partitioned into a sublimation process, where the individual components of the crystal are brought into the gas phase at infinite distance, followed by hydration, upon which each ion is surrounded by interacting water molecules (Scheme 2).
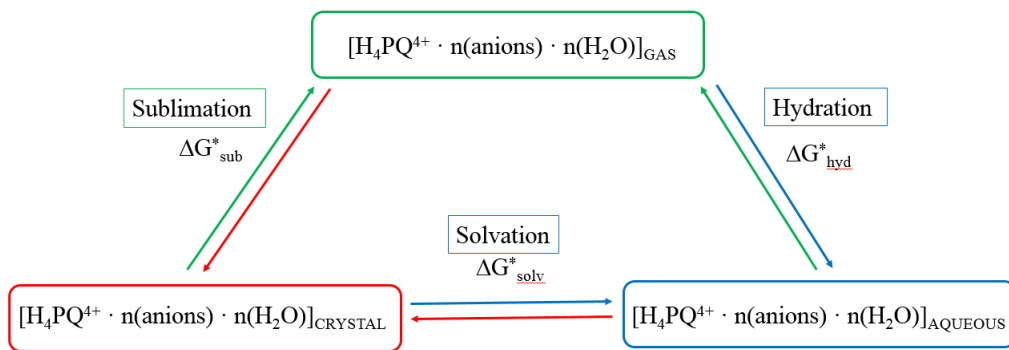
Scheme 2.

Altogether, sublimation, hydration and solvation form a closed thermodynamic cycle, meaning that the following equality holds true:

$$\Delta G^*_{solv} = \Delta G^*_{hyd} + \Delta G^*_{sub} \qquad (2)$$

Here, ΔG^*_{hyd} and ΔG^*_{sub} refer to hydration and sublimation energies. Moreover, assuming as unitary any activity coefficient, it has been shown[58] that the Gibbs free energies of solvation are related to the experimental solubilities, S:

$$\Delta G^*_{solv} = -RT\ln(S \cdot V_m) \qquad (3)$$

V_m (the crystalline molar volume) being equal to:

$$V_m = N_A V_{cell}/(Z \cdot Z') \qquad (4)$$

N_A is the Avogadro's constant, V_{cell} the real cell volume, and Z and Z' the number of asymmetric units in the unit cell, and the number of molecules in the asymmetric unit. Thus, V_m just represents the average volume per molecule in the crystal. Putting together (2) and (3), ΔG^*_{sub} can be computed directly from the experimental estimates of S_{exp}, once that a reasonable estimate of ΔG^*_{hyd} is known (Table 3). This method has been recently applied with success to first-principles prediction of aqueous solubilities of small organic molecules.[56,65] In the present case, results for transformations taking place at $T = 25\ °C$ are shown in Table S16 SI. It turns out that the free energy of solvation is invariably small and positive, as it can be expected from the low solubilities of PQ salts (Section 3.3). Moreover, the free energies of sublimation correlate well with the corresponding lattice energies (Figure S12 SI), *i.e.* the most negative E_{coh}'s correspond to the highest sublimation free energies, and *vice versa*. This guarantees that the present predictions of thermodynamic quantities, though clearly approximate, are accurate enough to provide reliable results on relative grounds.

Table 4. Comparison of relevant outcomes of quantum simulations, measured solubilities and thermodynamic state functions for the title compounds.

Substance	S / mol·L^{-1} [a]	ΔS°_{solv} / kJ·mol^{-1}·K^{-1}	ΔG°_{sub} [b]/ kJ·mol^{-1}	η(anions) /eV [c]	C_{pack} [d]
PPT	0.0104	2.02	3543.8	3.20	70.6
PHS	0.0017	2.09	5326.8	2.91	75.8
PTT	0.0134	0.51	3162.3	2.96	67.3
PBT	0.0209	2.04	3756.4	2.02	70.4
PN	0.0045	1.11	3263.4	3.55	70.5

[a] Average solubility in water and AcOH 1 M at T = 25 ºC (298 K). See also Tables S11–S12 SI.

[b] Refer to Section S8.2 SI to see how ΔG°_{sub} are estimated from ΔG^{*}_{sub}.

[c] Chemical hardness (in eV), defined as the average energy of the frontier orbitals according to $\eta = (\varepsilon_{LUMO} - \varepsilon_{HOMO})/2$, under the assumption that the Koopmans' theorem is valid. Following Pearson,[66] η's of anions at their optimized geometries were estimated from the corresponding neutral radicals.

[d] Packing coefficient. It is defined as the ratio between the total volume occupied by molecules, in turn computed as the usual superposition of van der Waals hard spheres, and the total cell volume. C_{pack} represents the percent amount of space that is actually occupied within the crystal structure.

The standard entropy of solvation, ΔS°_{solv}, can be also estimated from the corresponding sublimation entropy, ΔS°_{sub}, if the equality $\Delta S^{\circ}_{solv} \approx \Delta S^{\circ}_{sub}$ holds true. Such a hypothesis implies that the difference of entropy between the gas phase and the solution is small, or, equivalently, that the entropy changes associated to both (crystal $\rightarrow$ gas) and (crystal $\rightarrow$ solution) processes should bear similar magnitudes. This condition is certainly verified for ideal dilute solutions, *i.e.* for example *in vivo*, where the drug concentration ranges from nM (in the cytoplasm) up to µM (in the digestive vacuole).[20] As for the present measurements (Tables S11 and S12 SI), where concentrations are of the mM order, the assumption of ideal behaviour can be still probably accepted with a reasonable level of confidence. A full description of the procedure exploited to estimate ΔS°_{sub} (and thus ΔS°_{solv}), based on the recipe suggested by Palmer and co–workers,[58] can be found in Section S8.2 SI. Table 4 summarizes the most important outcomes of statistical thermodynamic and quantum simulations, relating them to the solubility of PQ salts in standard ambient conditions (T = 298 K, p = 1 bar), as they are usually taken as suitable thermodynamic reference.

The solvation entropies of PHS, PPT and PBT have the same magnitude (Table 4). However, their solubilities are very different. Moreover, PTT is characterized by a ΔS°_{solv} four times smaller than PHS and PPT, though it is more soluble than both are. This means that the entropy balance, by itself, poorly correlates with solubility. In the next Section, the trends in solubility are analysed from a more general perspective, taking also into account the Pearson's estimates for anionic chemical hardnesses (see Table 4).

4. Discussion

With the only exception of the PHS salt, there is a good linear correlation between the anion hardness (η) and the solubility of the title compounds in standard ambient conditions (Figure 4). In general, the lower the hardness of the counter–anion, the higher the solubility of the salt. This can be rationalized in the framework of the Hard and Soft Acids and Bases (HSAB) theory:[67] due to their very large positive charge, H_4PQ^{4+} species are expected to be hard acids, and tend to bound more tightly hard bases.
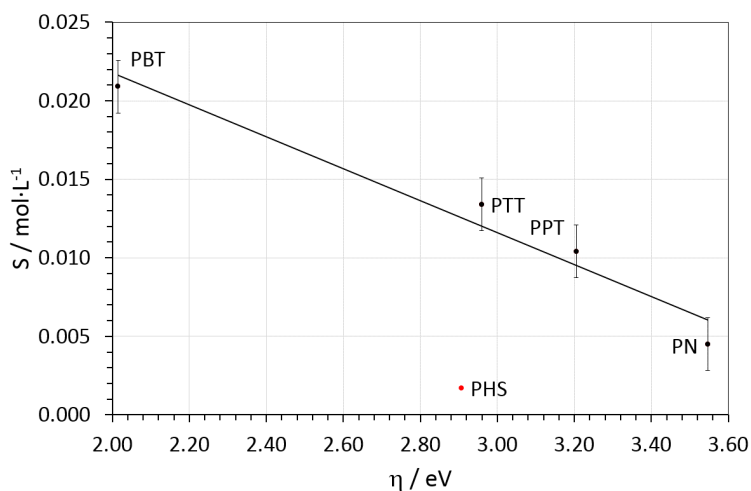
Figure 4. Linear correlation between the chemical hardness of the anions (η, eV) *vs.* the average solubility (S, mol·L^{-1}) of PQ salts at $T = 25\ °C$ (298 K). Tabular entries can be found in Table 4. The curve has equation $S = -0.010(1)\ \eta + 0.042(4)$, with $R^2 = 0.960$. Error bars correspond to 1 estimated standard deviation (e.s.d.), as derived from the least squares fitting. The red dot at the bottom corresponds to the hydrogen sulfate structure and it has been not included into the fitting.

The salt with the highest solubility, PQ bromide (PBT), contains indeed the softest anion (η = 2.02 eV, Table 4). Accordingly, the next ranking salt, triflate (PTT), has a higher η (2.96 eV). More interesting is the fact that, despite the sulfate salt PHS bears a comparable hardness (2.91 eV), is the least soluble on absolute grounds (Table 4). This is likely due to the intrinsically lower cohesion of the triflate crystal structure: PTT has the lowest packing coefficient and, accordingly, the lowest sublimation energy. Indeed, CF_3SO^{3-} is the largest anion in the whole set of structures here considered, and is definitely non-spherical. Thus, when paired with piperaquine, it is less able to occupy efficiently the available space. This complies well with the fact that, in PTT, H_4PQ^{4+} species prefer to assume a 'bent' conformation, more compact and symmetrical, rather than the most common 'stretched' one (Section 3.2). It is worth noting that PTT is also the only salt where two hydrogen bonds per PQ molecule involve neutral co–crystallized water molecules rather than charged anions

19

(Section 3.1). In contrast, in the bromide PBT, the higher solubility complies with a synergy of electronic (softness of Br⁻) and thermodynamic factors: the total hydration Gibbs free energy of Br⁻ ions is ≈ 100 kJ·mol⁻¹ more negative than that of the triflate ones (Table 3, Section 3.4), reflecting the higher molar amount of anions in the unit cell of PBT (Table 1 and Section S2.6 SI). Moreover, the Br⁻ ion has one of the highest entropic contributions to the solvation energy (Table 4), even though the latter accounts for less than 20 % of the overall ΔG^*_{solv} (Table S16 SI).

At the opposite extreme, PHS is the least soluble salt. Albeit being associated to an intermediate anion hardness (2.91 eV), PHS has the greatest sublimation free energy and the highest packing efficiency (Table 4). The very low solubility of this compound can be thus ascribed to a very high lattice stability. This latter, as in chloroquine[6] and organic salts in general,[49,68] is due to more favourable electrostatic interactions. A survey of Mulliken charges on oxygen and hydrogen atoms in organic anions (Table S17 SI), shows that HSO_4^- and SO_4^{2-} moieties bear the highest negative charge on their external O and OH groups (-2.51 and -3.42 e) with respect to all the other species here considered ($H_2PO_4^-$: -2.49 e; $CF_3SO_3^-$: -2.36 e; NO_3^-: -1.68 e). This implies that stronger electrostatic interactions are set up in PHS, which implies that, on average, different molecules are kept very close to each other in the crystal, as it is evident from the occurrence of a lot of short H···H contacts (Section 3.1). As expected, a stronger network of non–covalent interactions reflects into more negative cohesive energy (Table S14 SI) and larger ΔG^*_{sub} (Table 4).

The nitrate compound (PN) contains the hardest anion ($\eta = 3.55$ eV, Table 4), meaning that NO_3^- is expected to bear a greater affinity for protonated PQ than all the other anions here considered. Accordingly, the solubility of PN is very low at $T = 25$ ℃ (298 K, Table 4). However, it also rapidly increases with T, becoming even higher than those of PPT and PTT for $T > 40$ ℃ (313 K, Section 3.3, Figure 3). It should be remarked that PN is the only compound that does not contain co–crystallized water (Table 1) and, together with the most soluble PBT salt, it does not bear disordered groups (Sections 3.1 and S2.6 SI). On the contrary, PPT, PHS and PTT salts are all already partially disordered. Thus, their entropy gain upon solubilization is necessarily lower than expected, as our model for ΔS^o_{solv} completely neglects disorder effects. Disorder provides thus a rationale for the observed fast increment of solubilities of PBT and PN with T (Figure 3): the higher the temperature, the more favourable will be the entropy gain with respect to all the other structures upon solubilization.

The hydrogen phosphate salt (PPT) is associated to a more efficient packing and a higher sublimation free energy than PN (Table 4). Nevertheless, it is almost 3 times more soluble than PQ

nitrate at $T = 25\,°$ C, likely as $H_2PO_4^-$ anions have the most favourable hydration Gibbs free energy after the bromide ones (Table 3). This is easily explainable: at variance with NO_3^-, $H_2PO_4^-$ is amphiprotic, as it bears both acidic –OH functions (HB donors) and P=O free groups (HB acceptors). At the same time, however, PPT is also less soluble than the triflate PTT, according to the lower packing efficiency of the latter (see above).

5. Conclusions

In this work, five novel salts of piperaquine (PQ), a 4-aminoquinoline antiplasmodial employed in artemisinin[12]–combination therapies,[1,13,14] were synthesized and thoroughly characterized by crystallographic, spectroscopic and computational methods. The study was motivated by the need of more effective formulations of known antimalarial drugs, and the main aim was to understand how and why the measured solubility of PQ compounds depends on chemical, crystallographic and electronic degrees of freedom.

From a crystallographic viewpoint, solubility is related to structural and energetic properties of the lattice structure and crystal packing, but relevant solute–solvent interactions are known to be crucial factors as well. Accordingly, we found that the solubility of PQ cannot be related to just one specific structural or energetic aspect. Rather, it stems from the cooperative effects of several actors, even though the chemical hardness of the anions (η) seems to play a central role. According to the predictions of the HSAB theory, softer anions are generally associated to highly soluble salts. Only the hydrogen sulfate salt is totally off–trend, due to its exceptionally high lattice stability. At the same time, fully ordered compounds (bromide, nitrate), which experience a larger entropy gain upon solubilization, have solubilities that increase faster as T is raised with respect to salts bearing some kind of disorder (hydrogen phosphate, hydrogen sulfate, triflate). Other factors being similar, packing efficiency and crystal field strength become important, as for example the triflate compound is highly soluble at standard ambient conditions due to a lower packing coefficient, coupled to a less favourable number of charge-assisted hydrogen bonds per PQ molecule. On the contrary, parameters such as the solid-state conformation of protonated PQ, the nature of different $\pi\cdots\pi$ stacking modes, or the number and type of hydrogen bonds in the crystal, have no direct effect on the observed solubilities.

From the present results, it seems that a good strategy to increase the solubility of PQ salts be the coupling of the drug with soft anions, in the sense of the HSAB theory. Moreover, selecting crystalline phases with low intrinsic disorder, or not disordered at all, will likely result in formulations that are more soluble at higher temperature – which can have significant implications on transport

and storage of the active pharmaceutical ingredient. Studies of other crystalline piperaquine salts containing anions suitable for human administration will be carried out in the next future. Hopefully, they will pave the way toward more effective administration modes of the drug, increasing the current toolbox of strategies aimed at finely tuning its bioavailability.

Supporting Information Available. Effect of pH on the protonation state. X–ray diffraction analysis of PQ compounds. Procedures for solid–state quantum simulations. Stacking. Puckering parameters. Calibration procedure for the UV–vis measurements. UV–vis spectra. Quantum simulations: supplementary data. Cohesive energies and solubility. Thermodynamic analysis. Electronic parameters.

References

(1)   Davis, T. M. E.; Hung, T.; Sim, I.; Karunajeewa, H. a; Ilett, K. F. A Resurgent Antimalarial Drug. *Drugs* **2005**, *65* (1), 75–87.

(2)   Tärning, J. Piperaquine. Bioanalysis, Drug Metabolism and Pharmacokinetics, Göteborg University, 2007.

(3)   Hung, T. Y.; Davis, T. M. E.; Ilett, K. F.; Karunajeewa, H.; Hewitt, S.; Denis, M. B.; Lim, C.; Socheat, D. Population Pharmacokinetics of Piperaquine in Adults and Children with Uncomplicated Falciparum or Vivax Malaria. *Br. J. Clin. Pharmacol.* **2004**, *57* (3), 253–262.

(4)   Hung, T. Y.; Davis, T. M. E.; Ilett, K. F. Measurement of Piperaquine in Plasma by Liquid Chromatography with Ultraviolet Absorbance Detection. *J. Chromatogr. B Anal. Technol. Biomed. Life Sci.* **2003**, *791* (1–2), 93–101.

(5)   Macetti, G.; Rizzato, S.; Beghi, F.; Silvestrini, L.; Lo Presti, L. On the Molecular Basis of the Activity of the Antimalarial Drug Chloroquine: EXAFSassisted DFT Evidence of a Direct Fe–N Bond with Free Heme in Solution. *Phys. Scr.* **2016**, *91*, 023001.

(6)   Macetti, G.; Loconte, L.; Rizzato, S.; Gatti, C.; Lo Presti, L. Intermolecular Recognition of the Antimalarial Drug Chloroquine: A Quantum Theory of Atoms in Molecules-Density Functional Theory Investigation of the Hydrated Dihydrogen Phosphate Salt from the 103 K X-Ray Structure. *Cryst. Growth Des.* **2016**, *16* (10), 6043–6054.

(7)   Leed, A.; DuBay, K.; Ursos, L. M. B.; Sears, D.; De Dios, A. C.; Roepe, P. D. Solution Structures of Antimalarial Drug - Heme Complexes. *Biochemistry* **2002**, *41* (32), 10245–10255.

(8)   Dascombe, M. J.; Drew, M. G. B.; Morris, H.; Wilairat, P.; Auparakkitanon, S.; Moule, W. A.; Alizadeh-Shekalgourabi, S.; Evans, P. G.; Lloyd, M.; Dyas, A. M.; et al. Mapping Antimalarial Pharmacophores as a Useful Tool for the Rapid Discovery of Drugs Effective in Vivo: Design, Construction, Characterization, and Pharmacology of Metaquine. *J. Med. Chem.* **2005**, *48* (17), 5423–5436.

(9)   Walczak, M. S.; Lawniczak-Jablonska, K.; Wolska, A.; Sienkiewicz, A.; Suárez, L.; Kosar, A. J.; Bohle, D. S. Understanding Chloroquine Action at the Molecular Level in Antimalarial Therapy: X-Ray Absorption Studies in Dimethyl Sulfoxide Solution. *J. Phys. Chem. B* **2011**, *115* (5), 1145–1150.

(10)   Portela, C.; Afonso, C. M. M.; Pinto, M. M. M.; Ramos, M. J. Receptor-Drug Association Studies in the Inhibition of the Hematin Aggregation Process of Malaria. *FEBS Lett.* **2003**,

547 (1–3), 217–222.

(11) Asghari-Khiavi, M.; Vongsvivut, J.; Perepichka, I.; Mechler, A.; Wood, B. R.; McNaughton, D.; Bohle, D. S. Interaction of Quinoline Antimalarial Drugs with Ferriprotoporphyrin IX, a Solid State Spectroscopy Study. *J. Inorg. Biochem.* **2011**, *105* (12), 1662–1669.

(12) Saleh, G.; Soave, R.; Lo Presti, L.; Destro, R. Progress in the Understanding of the Key Pharmacophoric Features of the Antimalarial Drug Dihydroartemisinin: An Experimental and Theoretical Charge Density Study. *Chem. - A Eur. J.* **2013**, *19* (10), 3490–3503.

(13) Ashley, E. A.; Krudsood, S.; Phaiphun, L.; Srivilairit, S.; McGready, R.; Leowattana, W.; Hutagalung, R.; Wilairatana, P.; Brockman, A.; Looareesuwan, S.; et al. Randomized, Controlled Dose-Optimization Studies of Dihydroartemisinin-Piperaquine for the Treatment of Uncomplicated Multidrug-Resistant Falciparum Malaria in Thailand. *J. Infect. Dis.* **2004**, *190* (10), 1773–1782.

(14) Piyaphanee, W.; Krudsood, S.; Tangpukdee, N.; Thanachartwet, W.; Silachmroon, U.; Phophak, N.; Duangdee, C.; Haoharn, O.; Faithong, S.; Wilairatana, P.; et al. Emergence and Clearance of Gametocytes in Uncomplicated Plasmodium Falciparum Malaria. *Am. J. Trop. Med. Hyg.* **2006**, *74* (3), 432–435.

(15) Duru, V.; Witkowski, B.; Ménard, D. Review Article Plasmodium Falciparum Resistance to Artemisinin Derivatives and Piperaquine: A Major Challenge for Malaria Elimination in Cambodia. *Am. J. Trop. Med. Hyg.* **2016**, *95* (6), 1228–1238.

(16) Amato, R.; Pearson, R. D.; Almagro-Garcia, J.; Amaratunga, C.; Lim, P.; Suon, S.; Sreng, S.; Drury, E.; Stalker, J.; Miotto, O.; et al. Origins of the Current Outbreak of Multidrug-Resistant Malaria in Southeast Asia: A Retrospective Genetic Study. *Lancet Infect. Dis.* **2018**, *18* (3), 337–345.

(17) Slater, A. F.; Swiggard, W. J.; Orton, B. R.; Flitter, W. D.; Goldberg, D. E.; Cerami, A.; Henderson, G. B. An Iron-Carboxylate Bond Links the Heme Units of Malaria Pigment. *Proc. Natl. Acad. Sci.* **1991**, *88* (2), 325–329.

(18) Olafson, K. N.; Ketchum, M. A.; Rimer, J. D.; Vekilov, P. G. Mechanisms of Hematin Crystallization and Inhibition by the Antimalarial Drug Chloroquine. *Proc. Natl. Acad. Sci.* **2015**, *112* (16), 4946–4951.

(19) De Dios, A. C.; Tycko, R.; Ursos, L. M. B.; Roepe, P. D. NMR Studies of Chloroquine-Ferriprotoporphyrin IX Complex. *J. Phys. Chem. A* **2003**, *107* (30), 5821–5825.

(20) Warhurst, D. C.; Craig, J. C.; Adagu, I. S.; Guy, R. K.; Madrid, P. B.; Fivelman, Q. L.

Activity of Piperaquine and Other 4-Aminoquinoline Antiplasmodial Drugs against Chloroquine-Sensitive and Resistant Blood-Stages of Plasmodium Falciparum. *Biochem. Pharmacol.* **2007**, *73* (12), 1910–1926.

(21)   Serajuddin, A. T. M. Salt Formation to Improve Drug Solubility. *Adv. Drug Deliv. Rev.* **2007**, *59* (7), 603–616.

(22)   Paulekuhn, G. S.; Dressman, J. B.; Saal, C. Trends in Active Pharmaceutical Ingredient Salt Selection Based on Analysis of the Orange Book Database. *J. Med. Chem.* **2007**.

(23)   Williams, H. D.; Trevaskis, N. L.; Charman, S. A.; Shanker, R. M.; Charman, W. N.; Pouton, C. W.; Porter, C. J. H. Strategies to Address Low Drug Solubility in Discovery and Development. *Pharmacol. Rev.* **2013**.

(24)   Stahl, P. H.; Wermuth, C. G.; International Union of Pure and Applied Chemistry. *Handbook of Pharmaceutical Salts : Properties, Selection, and Use*; 2008.

(25)   Committee for Medicinal Products for Human Use. Assessment Report: Eurartesim; INN: Piperaquine Tetraphosphate/Dihydroartemisinin, Procedure No.: EMEA/H/C/1199. **2011**, *44* (June).

(26)   Lundberg, J. O.; Carlstörm, M.; Larsen, F. J.; Weitzberg, E. Roles of Dietary Inorganic Nitrate in Cardiovascular Health and Disease. *Cardiovascular Research*. 2011.

(27)   Butler, A. R.; Feelisch, M. Therapeutic Uses of Inorganic Nitrite and Nitrate: From the Past to the Future. *Circulation*. 2008.

(28)   Dhanya, S.; Lal, K.; Reena, S. In Silico Toxicology - A Tool for Early Safety Evaluation of Drug. *J Bioinform, Genomics, Proteomics* **2018**, *3* (1), 1030–1041.

(29)   Merlot, C. Computational Toxicology-a Tool for Early Safety Evaluation. *Drug Discovery Today*. 2010.

(30)   Wang, Q.; Huang, Y. M.; Ma, X. L.; Li, S. S.; Li, H. X-Ray Powder Diffraction Data for Piperaquine, C29H32Cl2N6. *Powder Diffr.* **2014**, *29* (1), 46–47.

(31)   Bruker. APEX2 Software Reference Manuals. Madison, Wisconsin, USA 2014.

(32)   Krause, L.; Herbst-Irmer, R.; Sheldrick, G. M.; Stalke, D. Comparison of Silver and Molybdenum Microfocus X-Ray Sources for Single-Crystal Structure Determination. *J. Appl. Crystallogr.* **2015**, *48* (1), 3–10.

(33)   Sheldrick, G. M. Crystal Structure Refinement with SHELXL. *Acta Crystallogr. Sect. C Struct. Chem.* **2015**, *71* (Md), 3–8.

(34)   Allen, F. H.; Bruno, I. J. Bond Lengths in Organic and Metal-Organic Compounds Revisited:

X - H Bond Lengths from Neutron Diffraction Data. *Acta Crystallogr. Sect. B Struct. Sci.* **2010**, *66* (3), 380–386.

(35) Macrae, C. F.; Bruno, I. J.; Chisholm, J. A.; Edgington, P. R.; McCabe, P.; Pidcock, E.; Rodriguez-Monge, L.; Taylor, R.; Van De Streek, J.; Wood, P. A. Mercury CSD 2.0 - New Features for the Visualization and Investigation of Crystal Structures. *J. Appl. Crystallogr.* **2008**, *41* (2), 466–470.

(36) Daneshfar, A.; Vafafard, S. Solubility of Chloroquine Diphosphate and 4,7-Dichloroquinoline in Water, Ethanol, Tetrahydrofuran, Acetonitrile, and Acetone from (298.2 to 333.2) K. *J. Chem. Eng. Data* **2009**, *54* (8), 2170–2173.

(37) Dovesi, R.; Saunders, V. R.; Roetti, C.; Orlando, R.; Zicovich-Wilson, C. M.; Pascale, F.; Civalleri, B.; Doll, K.; Harrison, N. M.; Bush, I. J.; et al. CRYSTAL 14: User's Manual. *Univ. Torino, Torino* **2016**, 1–382.

(38) Zhao, Y.; Truhlar, D. G. The M06 Suite of Density Functionals for Main Group Thermochemistry, Thermochemical Kinetics, Noncovalent Interactions, Excited States, and Transition Elements: Two New Functionals and Systematic Testing of Four M06-Class Functionals and 12 Other Function. *Theor. Chem. Acc.* **2008**, *120* (1–3), 215–241.

(39) Gatti, C.; Saunders, V. R.; Roetti, C. Crystal Field Effects on the Topological Properties of the Electron Density in Molecular Crystals: The Case of Urea. *J. Chem. Phys.* **1994**, *101* (12), 10686–10696.

(40) Apra, E.; Causa, M.; Prencipe, M.; Dovesi, R.; Saunders, V. R. On the Structural Properties of NaCl: An Ab Initio Study of the B1\mbox{-}{B}2 Phase Transition. *J. Phys. Condens. Mat.* **1993**, *5* (18), 2969–2976.

(41) Heyd, J.; Peralta, J. E.; Scuseria, G. E.; Martin, R. L. Energy Band Gaps and Lattice Parameters Evaluated with the Heyd-Scuseria-Ernzerhof Screened Hybrid Functional. *J. Chem. Phys.* **2005**, *123* (17).

(42) Zicovich-Wilson, C. M.; Bert, A.; Roetti, C.; Dovesi, R.; Saunders, V. R. Characterization of the Electronic Structure of Crystalline Compounds through Their Localized Wannier Functions. *J. Chem. Phys.* **2002**, *116* (3), 1120–1127.

(43) Nada, R.; Catlow, C. R. A.; Pisani, C.; Orlando, R. An Ab-Initio Hartree-Fock Perturbed-Cluster Study of Neutral Defects in Lif. *Model. Simul. Mater. Sci. Eng.* **1993**, *1* (2), 165–187.

(44) Doll, K.; Stoll, H. Ground-State Properties of Heavy Alkali Halides. *Phys. Rev. B* **1998**, *57* (8), 4327–4331.

(45)   Lo Presti, L.; Soave, R.; Longhi, M.; Ortoleva, E. Conformational Polymorphism in a Schiff-Base Macrocyclic Organic Ligand: An Experimental and Theoretical Study. *Acta Crystallogr. B.* **2010**, *66* (Pt 5), 527–543.

(46)   Lo Presti, L.; Ellern, A.; Destro, R.; Lunelli, B. Effect of Methoxy Substituents on the Structural and Electronic Properties of Fluorinated Cyclobutenes: A Study of Hexafluorocyclobutene and Its Vinyl Methoxy Derivatives by XRD and Periodic DFT Calculations. *J. Phys. Chem. A* **2009**, *113* (13), 3186–3196.

(47)   Lo Presti, L. On the Significance of Weak Hydrogen Bonds in Crystal Packing: A Large Databank Comparison of Polymorphic Structures. *CrystEngComm* **2018**, *20* (39), 5976–5989.

(48)   Gavezzotti, A.; Lo Presti, L. Theoretical Study of Chiral Carboxylic Acids. Structural and Energetic Aspects of Crystalline and Liquid States. *Cryst. Growth Des.* **2015**, *15* (8), 3792–3803.

(49)   Gavezzotti, A.; Rizzato, S.; Lo Presti, L. The TACO Puzzle: A Phase-Transition Mystery Revisited. *Cryst. Growth Des.* **2018**.

(50)   Boys, S. F.; Bernardi, F. The Calculation of Small Molecular Interactions by the Differences of Separate Total Energies. Some Procedures with Reduced Errors. *Mol. Phys.* **1970**, *19* (4), 553–566.

(51)   Frisch, M. J. . et al. Official Gaussian 09 Literature Citation. *Gaussian 09, Revis. D.01; Gaussian Inc. Wallingford CT J.* **2009**.

(52)   Marenich, A. V; Cramer, C. J.; Truhlar, D. G. Unviersal Solvation Modle Based on Solute Electron Density and a Contiuum Model of the Solvent Defind by the Bulk Dielectric Constant and Atomic Surface Tensions. *J. Phys. Chem. B.* **2009**, *113*, 6378–6396.

(53)   Spackman, M. A.; McKinnon, J. J. Fingerprinting Intermolecular Interactions in Molecular Crystals. *CrystEngComm* **2002**, *4* (66), 378–392.

(54)   Wolff, S. K.; Grimwood, D. J.; McKinnon, J. J.; Turner, M. J.; Jayatilaka, D.; Spackman, M. A. CrystalExplorer. University of Western Australia 2012.

(55)   Shannon, R. Revised Effective Ionic Radii and Systematic Studies of Interatomic Distances in Halides and Chalcogenides. *Acta Cristal. Sect. A Found. Adv.* **1976**, *32*, 751–767.

(56)   Palmer, D. S.; Llinàs, A.; Morao, I.; Day, G. M.; Goodman, J. M.; Glen, R. C.; Mitchell, J. B. O. Predicting Intrinsic Aqueous Solubility by a Thermodynamic Cycle. *Mol. Pharm.* **2008**, *5* (2), 266–279.

(57) S. de Moraes, L.; Edwards, D.; Florence, A. J.; Johnston, A.; Johnston, B. F.; Morrison, C. A.; Kennedy, A. R. Aqueous Solubility of Organic Salts. Investigating Trends in a Systematic Series of 51 Crystalline Salt Forms of Methylephedrine. *Cryst. Growth Des.* **2017**, *17* (6), 3277–3286.

(58) Skyner, R. E.; McDonagh, J. L.; Groom, C. R.; Van Mourik, T.; Mitchell, J. B. O. A Review of Methods for the Calculation of Solution Free Energies and the Modelling of Systems in Solution. *Phys. Chem. Chem. Phys.* **2015**, *17* (9), 6174–6191.

(59) Black, S. N.; Collier, E. A.; Davey, R. J.; Roberts, R. J. Structure, Solubility, Screening, and Synthesis of Molecular Salts. *J. Pharm. Sci.* **2007**, *96* (5), 1053–1068.

(60) Ochterski, J. W. Thermochemistry in *Gaussian*. *Gaussian Inc* **2000**, 1–19.

(61) Lo Presti, L.; Sist, M.; Loconte, L.; Pinto, A.; Tamborini, L.; Gatti, C. Rationalizing the Lacking of Inversion Symmetry in a Noncentrosymmetric Polar Racemate: An Experimental and Theoretical Study. *Cryst. Growth Des.* **2014**, *14* (11), 5822–5833.

(62) Ben-Naim, A.; Marcus, Y.; Palmer, D. S.; Llinàs, A.; Morao, I.; Day, G. M.; Goodman, J. M.; Glen, R. C.; Mitchell, J. B. O.; Ben-Naim, A.; et al. Solvation Thermodynamics of Nonionic Solutes. *J. Chem. Phys.* **1984**, *81* (4), 2016–2027.

(63) Misin, M.; Fedorov, M. V.; Palmer, D. S. Hydration Free Energies of Molecular Ions from Theory and Simulation. *J. Phys. Chem. B* **2016**, *120* (5), 975–983.

(64) Marcus, Y. Thermodynamics of Solvation of Ions. Part 5.—Gibbs Free Energy of Hydration at 298.15 K. *J. Chem. Soc. Faraday Trans.* **1991**, *87* (18), 2995–2999.

(65) Palmer, D. S.; McDonagh, J. L.; Mitchell, J. B. O.; van Mourik, T.; Fedorov, M. V; Mourik, T. Van; Fedorov, M. V. First-Principles Calculation of the Intrinsic Aqueous Solubility of Crystalline Druglike Molecules. *J. Chem. Theory Comput.* **2012**, *8* (9), 3322–3337.

(66) Pearson, R. G. Absolute Electronegativity and Hardness: Application to Inorganic Chemistry. *Inorg. Chem.* **1988**, *27* (4), 734–740.

(67) Atkins, P.; Overton, T.; Rourke, J.; Weller, M.; Armstrong, F. *Shriver and Atkins' Inorganic Chemistry*; Oxford University Press, 2010.

(68) Destro, R.; Ortoleva, E.; Soave, R.; Loconte, L.; Lo Presti, L. Detection and Kinetics of the Single-Crystal to Single-Crystal Complete Transformation of a Thiiranium Ion into Thietanium Ion. *Phys. Chem. Chem. Phys.* **2009**, *11* (33), 7181.

For Table of Contents use only
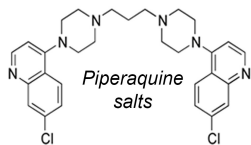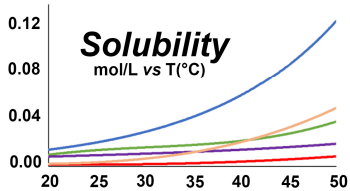
Synopsis: *The solubility of salts of the antiplasmodial piperaquine depends on the mutual chemical affinity between the drug and its counter ions.*